Rainfall spatial-heterogeneity accelerates landscape evolution processes

Geomorphology 390 (2021) 107863

Contents lists available at ScienceDirect

Geomorphology

journal homepage: www.elsevier.com/locate/geomorph

Rainfall spatial-heterogeneity accelerates landscape evolution processes

Nadav Peleg [a,*], Chris Skinner [b], Jorge Alberto Ramirez [c], Peter Molnar [a]

[a] Institute of Environmental Engineering, ETH Zurich, Zurich, Switzerland
[b] Energy and Environment Institute, University of Hull, Hull, UK
[c] Geography Department, Université du Québec à Montréal, Montréal, Québec, Canada

ARTICLE INFO

Article history:
Received 10 March 2021
Received in revised form 15 July 2021
Accepted 15 July 2021
Available online 20 July 2021

Keywords:
Rainfall spatial properties
Storm characteristics
Landscape evolution model
Gully erosion
Enhanced erosion rates
Catchment morphology

ABSTRACT

Catchment hydro-morphological response is mainly conditioned on rainfall properties, such as rainfall intensity, storm duration and frequency, and the timing of these events. Rainfall spatial variability is likewise a major determinant affecting streamflow, erosion, and sediment transport, and is explored largely in the context of heavy rain triggering floods and fast morphological changes on hillslopes and in channels. In this study, we examine how the spatial structure of rainfall influences landscape evolution at the catchment scale over hundreds of years. To achieve this, multiple realizations of hourly rainfall fields, each differing only by their spatial distribution but identical in all other respects, were simulated using a weather generator. The impact of storm spatial-heterogeneity on the catchment morphology was then assessed with a landscape evolution model (CAESAR-Lisflood). A virtual "open-book" type catchment was used for this numerical experiment. The mean streamflow and low-flows remained the same while the magnitude of the annual peak streamflow increased by up to 12% in response to higher rainfall spatial heterogeneity. However, the erosion and deposition rates significantly increased (up to 50%) and the net erosion and deposition areas changed (increased by up to 9% and decreased by 13.5%, respectively) when the rain became less uniform in space. Furthermore, new gullies were found to be longer, deeper, and more branched in response to increased rainfall heterogeneity. The results suggest that heterogeneity in rainfall spatial patterns speeds up landscape development, even when rainfall volumes and temporal structures are the same. This implies that the spatial structure of rainfall may have more of an influence on catchment morphology at long time scales than previously thought.

1. Introduction

Rainfall is a crucial component in many hydrological processes, and hydro-morphological systems are highly sensitive to it (Fekete et al., 2004). Rainfall not only controls streamflow levels but also is the main trigger for different types of floods (Merz and Bloschl, 2003). For example, pluvial floods in urban and dry environments often initiate with a short (minute-scale) and intense burst of rainfall (Acosta-Coll et al., 2018); in wet climates, flood events can be caused by long-lasting (day-scale) storms with a large volume of rainfall (Villarini et al., 2010); and in mountainous areas, flooding can result from rain-on-snow events (Jones and Perkins, 2010). Rainfall is also known to be the main trigger for landslides (Iverson, 2000; Leonarduzzi and Molnar, 2020), debris flows (Guzzetti et al., 2008; Marra et al., 2016), and rapid erosion and transport of sediment (Valentin et al., 2005; Xu et al., 2015).

Due to its importance, the properties of rainfall are thoroughly researched. For example, increased frequency of storms implies wetter conditions preceding the storms, which can act to boost streamflow and sediment erosion (Gallart et al., 2005; Salvadori and De Michele, 2006). On the same note, comparisons between storms with the same rainfall amounts reveal that longer-lasting storms can be more efficient in saturating the soil, hence enhancing streamflow and triggering more landslides (Montgomery et al., 1997; Struthers et al., 2007; Tarolli et al., 2011). The temporal properties of rainfall and their effect on hydro-morphological systems have been investigated for many years, with most of the studies focusing on aspects of intensity, duration, and frequency of rainfall (Koutsoyiannis et al., 1998; Sivapalan and Bloschl, 1998; Willems, 2000; Borga et al., 2014; among many others).

For most catchments, the temporal properties of rainfall are more important in affecting the hydro-morphological response of the system than the spatial properties of rainfall (Robinson and Sivapalan, 1997; Tucker and Bras, 2000; Gayer et al., 2019). However, the spatial dimension of rainfall cannot be overlooked as its contribution is still meaningful (Singh, 1997). For example, rainfall spatial variability was found to explain 20–30% of the variability in flood volumes in the city of Luzern (Peleg et al., 2017a), and its contribution can be even higher for rural catchments (Zhu et al., 2018).

* Corresponding author at: Stefano-Franscini-Platz 5, 8093 Zurich, Switzerland.
E-mail address: nadav.peleg@sccer-soe.ethz.ch (N. Peleg).

https://doi.org/10.1016/j.geomorph.2021.107863
0169-555X/

Different aspects of the hydro-morphological response to rainfall spatial properties were previously researched, mainly using numerical models (e.g. Menabde and Sivapalan, 2001; Dodov and Foufoula-Georgiou, 2005; Mejia and Moglen, 2010; Baartman et al., 2013; Coulthard and Skinner, 2016; Skinner et al., 2020). It has been shown that trajectories of storms with respect to the dominant aggregation of flow through the river network can highly influence the streamflow (Morin et al., 2006; Chang, 2007; van Werkhoven et al., 2008; Yakir and Morin, 2011). Other studies demonstrate that storm velocity can have a major influence on streamflow enhancement (lower velocity, higher impact; see Ogden et al., 1995; Singh, 1997; Paschalis et al., 2014) and landslide initiation (Guthrie et al., 2010). Changes to the storm profile, e.g. due to temperature increase in a warmer climate, can result in faster and stronger hydro-morphological response, even if the rainfall amounts are almost the same (Peleg et al., 2020).

Studying the hydro-morphological response to rainfall spatial properties is not a trivial task as it requires either data of rainfall fields from remote sensing systems (if observed data are analyzed) or from numerical simulations (if different rainfall scenarios are explored). For most small-to-medium size catchments, the data should be at sub-hourly and (sub-)kilometer scales to match the hydro-morphological response in time and space (Ochoa-Rodriguez et al., 2015; Coulthard and Skinner, 2016; Cristiano et al., 2017). Most often, weather radars are used to obtain observed rainfall fields, and Convective Permitting Models (Prein et al., 2015) or gridded rainfall generator models (Paschalis et al., 2013; Peleg et al., 2017b; Singer et al., 2018; Papalexiou and Serinaldi, 2020) are used to simulate the rainfall at the high space-time resolution that is required. Few studies have so far explored the impacts of rainfall spatial properties on hydro-morphological systems. This is mainly due to the (i) lack of data available from weather radars; (ii) large amounts of computational storage required to save rain fields; (iii) complexity of running climate models; and (iv) high-computational resources needed to analyze multiple rain fields and to simulate the hydro-morphological processes at high resolution.

Due to the aforementioned limitations, previous studies were conducted mainly at the catchment scale and focused mostly on the hydro-morphological response to a single storm (e.g. Paschalis et al., 2014; Peleg et al., 2020). At the storm scale, we have adequate knowledge of how the properties of rainfall in space are impacting hydro-morphological processes. But a question that remains unanswered is what influences the spatial properties of rainfall have on catchment landscapes over long periods. By conducting a numerical experiment that utilizes a weather generator model to simulate rainfall fields, feeding these into a landscape evolution model to simulate the hydro-morphological response at the catchment-scale, and investigating the formation of stream morphology, erosion and deposition rates, and the pattern of gully formation under different scenarios of spatial rainfall properties, with the aim to contribute to answering the above question.

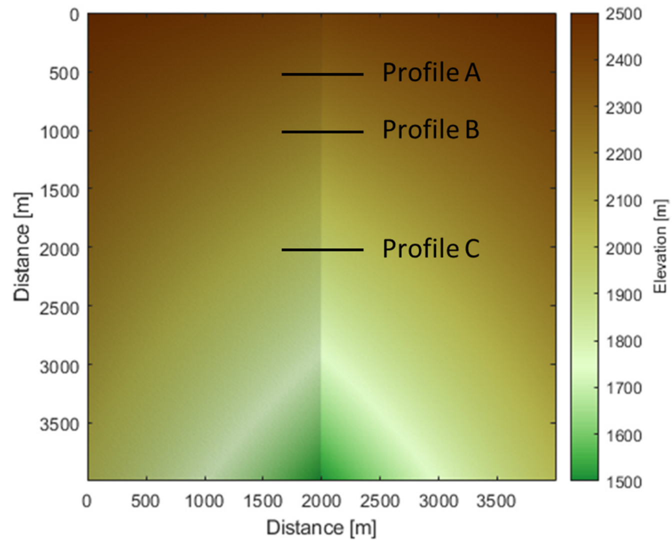

Fig. 2. A plan view of the virtual catchment.

2. Methods

The numerical experiment is illustrated in Fig. 1. In summary, we performed a rainfall simulation with multiple spatial scenarios over a long period of 300 years and then analyzed the differences in catchment hydro-morphological response. The study was conducted in a virtual environment, which is described in the next subsection.

2.1. Study area: a virtual catchment

Our virtual environment is a simplified and idealized “open-book” catchment (Fig. 2), which is commonly used in hydrological studies (e.g. Viglione et al., 2010; Volpi et al., 2013; Abdollahi et al., 2016). It is a simplified representation of a natural catchment that consists of a central channel and sloping planes delivering water to the channel, accounting for hillslopes and tributaries. We can completely control the hydro-geomorphic setup using our virtual catchment, such as fixing the depth to bedrock and not mixing different land-cover/land-use

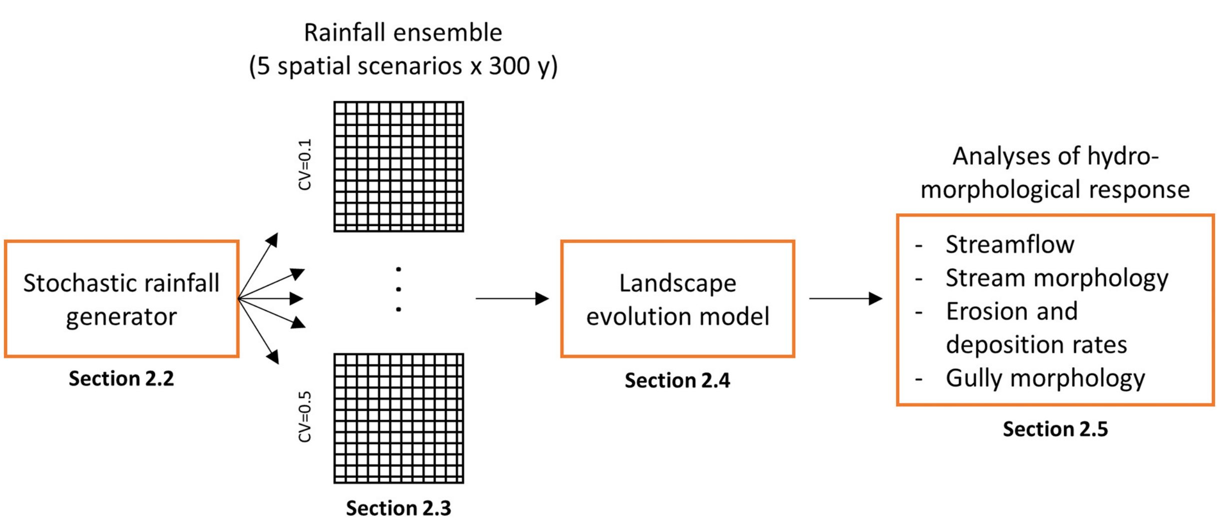

Fig. 1. A flowchart of the numerical experiment. CV is the rainfall spatial coefficient of variation.

types. By doing so, we can focus on a single process at a time, in this case, rainfall and hydro-morphological response, without worrying about the influence of other hydrological factors. Furthermore, the virtual catchment reduces the spatial heterogeneity of topography, which can dampen hydro-morphological responses. Consequently, an idealized virtual catchment can maximize the detection of landscape changes caused by different rainfall properties.

The domain size is 4000 m $\times$ 4000 m, with a grid size of 10 m $\times$ 10 m, a difference in elevation between 2500 m above reference level (top right and left corners, see Fig. 2) and 1500 m above reference level at the outlet of the catchment, and a strong slope of 22.5% along the main channel. Initially, a smooth terrain was generated. Next, it was randomly perturbed within $\pm$0.25 cm per grid cell, allowing the landscape to evolve differently between the two slopes. The depth to bedrock, defined as the layer where erosion can occur, varies from 10 m at the top of the catchment to 65 m next to the outlet (Fig. S1).

2.2. Stochastic rainfall model

Stochastic rainfall generator models are useful for simulating multiple realizations of a real- or pseudo-climate (Semenov and Barrow, 1997; Wilks and Wilby, 1999; Kilsby et al., 2007). The realizations simulated by gridded rainfall generators can be set to preserve the temporal statistics of the rainfall, such as storm frequencies and durations, and differ in how the rainfall intensities are spatially distributed within the domain. Here, we use the STREAP rainfall generator model (Paschalis et al., 2013; further developed by Peleg et al., 2017b; Peleg et al., 2019) that was used to generate high-resolution space-time rainfall fields in previous hydro-morphological impact studies (Peleg et al., 2020; Skinner et al., 2020).

The model generates rainfall fields in the following three steps (for more details see papers above). The first step is to draw the length of the storms and the dry intervals from a 4-parameter Johnson distribution. In the second step, a first-order autoregressive model is applied to each storm to simulate a time series of percentiles between 0 and 1 that represent the within-storm variability of mean rain intensity. The mean rainfall intensity is then computed using a 5-parameter Mixed Gamma and Generalized Pareto distribution. The time series of the mean rainfall intensity is transformed into space-time rainfall fields in the last step. The Fast Fourier Transform method is applied to simulate an isotropic Gaussian random field at the beginning of each storm that evolves spatially as the storm continues. Finally, a lognormal function is applied to convert the isotropic Gaussian fields into intermittent rainfall fields. The information needed for this transformation is the simulated mean rainfall over the domain and the spatial rainfall coefficient of variation, which is a model parameter:

$$R = LN^{-1}(U[G], \mu, \sigma) \tag{1}$$

where R is the intermittent rainfall field, LN^{-1} is the inverse cumulative lognormal distribution and $U[G]$ are the percentiles in space and time of the latent isotropic Gaussian field. μ and σ are the parameters of the lognormal distribution that are expressed as:

$$\mu = \log\left(\frac{IMF}{\sqrt{CV^2+1}}\right) \tag{2}$$

and

$$\sigma = \sqrt{\log\left(CV^2+1\right)} \tag{3}$$

where IMF is the mean rainfall intensity field at any given time step and CV is the rainfall spatial coefficient of variation, defined as the ratio of the standard deviation to the mean of the rainfall intensities over all grid cells at a given time step. The CV changes depending on the rainfall spatial scenario that is explained next.

2.3. Rainfall ensemble

We parameterized the rainfall generator to simulate an ensemble of 300 years at a high space-time resolution, so that the influence of the spatial structure of rainfall on the landscape can be examined on long timescales. First, a time series of the mean rainfall over the domain was simulated at hourly resolution (Section 2.3.1). Then, we simulate 5 realizations (with different CV) of gridded rainfall at 100-meter resolution using the above time series (Section 2.3.2). With this approach, we keep the same temporal structure of rainfall in every realization, i.e. the storms have the same rainfall volume, start time, duration and intra-storm temporal distribution of rainfall. The only difference between the realizations is the degree to which the distribution of rainfall in space is homogeneous. An example is provided in Movie S1, which shows the same synthetic storm (with mean intensity shown in Fig. S2) distributed over the virtual catchment with different degrees of spatial heterogeneity.

2.3.1. Simulating 300 years of rainfall at the domain scale

The rainfall generator was parameterized to simulate rainfall time series for a typical wet-climate in a mountainous region; the summer period in the Swiss Alps. The seasonality was fixed to remove the temporal variance in the hydro-morphological response to rainfall, i.e. all months were assumed to have identical rainfall statistics with a mean monthly rainfall of 140 mm (Fig. 3a). The duration of storms varies between 1 h and 75 h, with an average of 5 h (Fig. 3b). The model replicates the natural rainfall variability, as shown at the monthly (Fig. 3a) and annual scales (Fig. 3c). In the simulated 300 years, there was an adequate representation of years with low rainfall quantities (in the order of 1200 mm) and low amount of wet days (around 120 days per year), as well as years rich with rainfall (2300 mm and 190 wet days per year, Fig. 3c, d). The natural rainfall variability is also reflected in the rainfall extremes as maximum annual hourly rainfall amounts vary between 12 and 28 mm h^{-1} (Fig. 3e). The values of the model parameters used for simulating the 300 years rainfall time series are listed in Table S1.

2.3.2. Simulating rainfall spatial scenarios at 100-meter scale

Five different spatial scenarios (realizations) were generated. As explained in Section 2.2, the distribution of rainfall intensities depends directly on the spatial pattern of the latent Gaussian field. The ARMA parameters that control how the initial Gaussian field evolves in time were fixed in all realizations (Table 1) so that the same pattern of temporal change of the field is preserved. The scenarios are determined by one single parameter, the spatial coefficient of variation (CV), which varied between 0.1 and 0.5 for the 5 realizations (Table 1). This range of CV values represents plausible rainfall patterns in different locations and climates, as later discussed in Section 4.1.

Lower CV values produce more homogenous rainfall. Fig. 4 illustrates how changes in CV affect the spatial structure of the rainfall for the heavy storms. Heavy storms are defined as storms with rainfall intensities exceeding 18 mm h^{-1}; equivalent to the top 5% most intense storms. The rain field in each time step was centred on the moving location of the maximum rainfall intensity (a Lagrangian perspective, e.g. Peleg and Morin, 2012; Prein et al., 2017) and a composite of the mean rainfall intensities was computed. The lower CV value that was used (CV = 0.1, Fig. 4a) resulted in a homogenous rain field, while the highest CV value (CV = 0.5, Fig. 4c) produced a heterogeneous rain field with high local rainfall intensities. The main difference in the storm profile emerges among CV values of 0.1, 0.3 and 0.5, while storm profiles generated from CV values of 0.1 and 0.2, and of 0.4 and 0.5, were relatively similar (Fig. 4d). Examination of the spatial correlations in rainfall revealed that a CV value of 0.1 yielded more stratiform-like storms, while higher CV values resulted in more convective-like storms (May and Julien, 1998; Peleg et al., 2013; O and Foelsche, 2019b).

The parameters related to the advection in the storm, i.e. the storm velocity and storm direction (Table 1), were also held constant for all

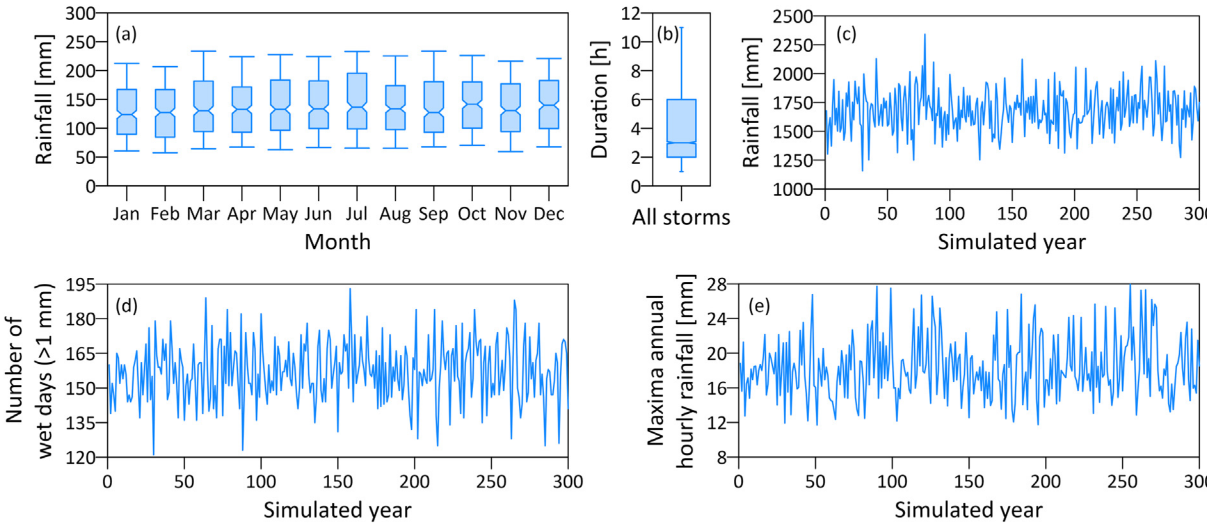

Fig. 3. Representation of the 300-year simulated rainfall: (a) boxplots representing the monthly rainfall (centre line is the median, box edges are the quartiles, and whiskers are the 10–90th percentiles); (b) a boxplot of the storm duration; (c) a time series of the annual rainfall amounts; (d) a time series of the number of wet days per year; and (e) a time series of the annual maxima rainfall.

Table 1
Properties of the storms and parameters of the stochastic rainfall generator model.

Parameter	Values	Units
Temporal resolution	1	h
Spatial resolution	100	m
Wet area ratio	1	–
Storm velocity	15	km h^{-1}
Storm direction	0	° from north
ARMA Gaussian field parameters	AR = 0.95, MA = 1	–
Coefficient of variation of spatial rainfall	0.1, 0.2, 0.3, 0.4, 0.5	–

storms in all realizations, following the concept and values as in Paschalis et al. (2014). This was done to remove the influence of storm trajectories on the hydro-morphological response, as previously mentioned. In spite of the fact that all the rainfall fields follow the same velocity and direction, the paths taken by heavy rainfall intensities over the virtual catchment change in time and space due to the stochasticity of the simulation and vary from storm to storm and within storms (see Movie S1). Therefore, the same distribution of rainfall intensity applies to all cells in the virtual catchment, i.e. the main channel and slopes are equally affected by heavy rainfall.

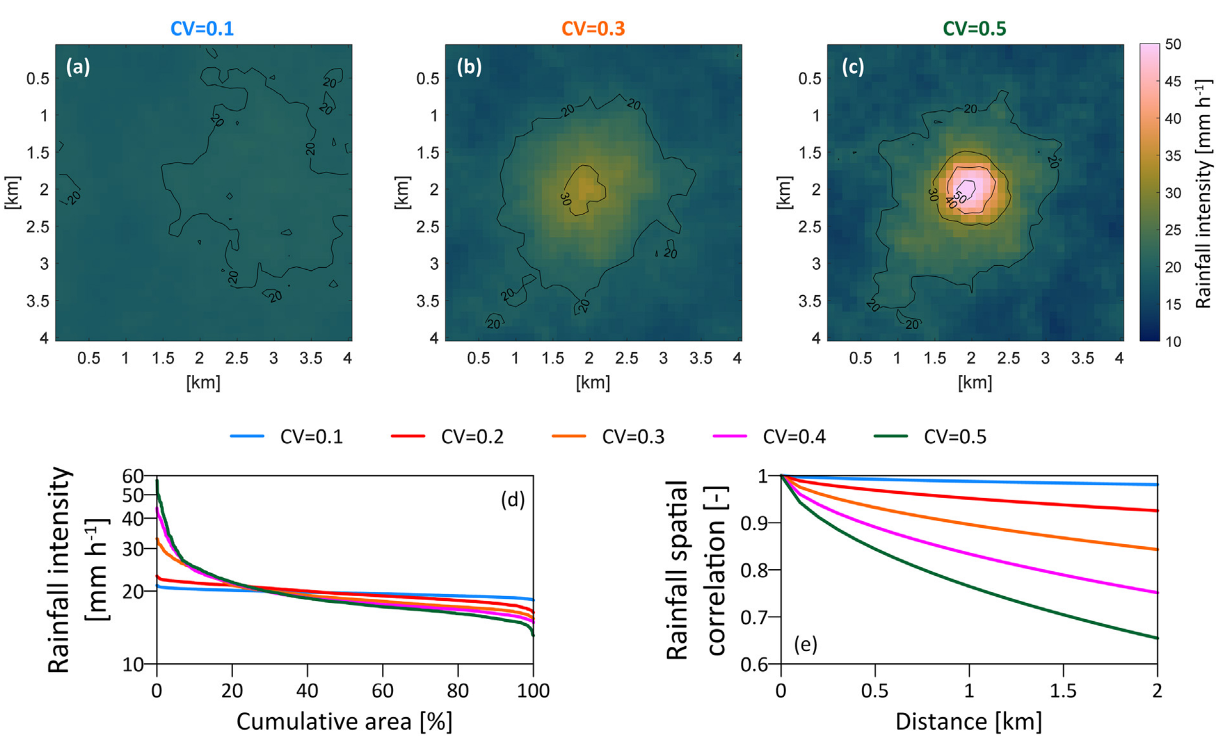

Fig. 4. The spatial patterns of simulated heavy storms with rainfall intensities larger than 18 mm h^{-1}. The hourly rainfall averages for different *CV* composited according to the moving location of the maximum rainfall intensity (a Lagrangian perspective) are presented in (a–c). The profile of the storms and the rainfall spatial correlations are presented in (d) and (e).

2.4. Landscape evolution model

CAESAR-Lisflood (Coulthard et al., 2013) was used to simulate the hydro-morphological processes. CAESAR-Lisflood is a grid-based landscape evolution model that has been widely used to simulate morphodynamic changes at small spatial scales (<1 km^2, Coulthard et al., 2012a; Hoober et al., 2017) and long temporal scales (>10^3 y, Hancock et al., 2010; Hancock et al., 2015; Coulthard and Van De Wiel, 2017). Furthermore, the model is particularly effective in exploring hydro-morphologic sensitivity to variations in rainfall spatial and temporal properties (Hancock, 2009; Hancock, 2012; Coulthard et al., 2012b; Hancock and Coulthard, 2012; Coulthard and Skinner, 2016; Hoober et al., 2017; Peleg et al., 2020; Skinner et al., 2020). TOPMODEL (Beven and Kirkby, 1979) is used for surface runoff computations and downstream routing is done with the LISFLOOD-FP model (Bates et al., 2010). The model was used in catchment mode using the Wilcock and Crowe (2003) formulation to compute fluvial erosion and sediment transport. We used version "1.9j" of the model without making any changes to the source code. Further information on the model can be found in Coulthard et al. (2013).

The model was set at the same temporal resolution as the rainfall fields, i.e. maximum dynamic time step of 1 h, to ensure the resulting landscape changes were not largely influenced by the dynamic time step. The spatial resolution was set to 10 m to make it possible to model erosion at a gully scale. The model parameters are listed in Table 2 and are the same for all grid cells in the catchment. The values of grainsize distribution and proportion, as well as the hydrological TOPMODEL parameters, are the same used by Peleg et al. (2020) for a CAESAR-Lisflood simulation of an Alpine catchment.

The initial conditions of the virtual catchment are far from equilibrium, and indeed, abrupt elevation changes were observed at the start of the simulation. Furthermore, at the beginning of the simulation, all of the grainsize distributions were the same along the channels. To avoid any bias due to these initial conditions, the first 150 years of the simulated model (out of 300 years in total) were considered as a "spin-up" period, allowing the landscape to approach dynamic equilibrium. The erosion and deposition rates and areas for the 300 years of simulation are presented for rainfall scenarios CV = 0.1 and CV = 0.5 in Fig. S3, and clearly show that dynamic equilibrium was achieved well within the first 150 years of simulation. The results of the analyses presented in Section 3 are based on the last 150 years of simulations, unless otherwise mentioned.

2.5. Analyses of hydro-morphological response

The hydro-morphological response to the changes in spatial rainfall distribution was examined in terms of changes in streamflow, stream morphology, erosion and deposition rates and areas, and gully development. Changes in streamflow are computed based on daily flow values and focus on three indices: (i) low flow, defined as the annual minimum 7-day streamflow; (ii) mean flow, defined as the mean streamflow of all days within a year with a flow larger than 0.5 m^3 s^{-1}; and (iii) peak streamflow, defined as the annual maximum daily flow.

The impacts on the stream morphology were assessed by examining the stream profiles in three locations along the main channel (Fig. 2). Monthly elevation differences of the entire catchment were used to compute erosion and deposition rates. The areas in which erosion and deposition occurred were also computed at monthly intervals; a grid cell was marked as "eroded" or "deposited" only if the change between two consecutive months was larger than 0.1 cm. The gully development (length and depth of erosion) was computed from the elevation changes at monthly scale. Additionally, information on side branching was determined using the Tokunaga stream order (Tokunaga, 1978; Pelletier and Turcotte, 2000). This is an extended classification of the Strahler ordering system, where the intersection of two first-order branches is denoted as '11,' the intersection of a first- and second-order branch as '12,' and so on.

Table 2
Parameters of the CAESAR-Lisflood model.

Parameter	Values	Units
Temporal resolution (maximal)	1	h
Spatial resolution	10	m
Grainsizes	0.0005, 0.003, 0.016, 0.04, 0.125, 0.2	m
Grainsize proportions (sum to 1)	0.1, 0.25, 0.25, 0.3, 0.05, 0.05	–
Suspended sediment fall velocity	0.066	m s^{-1}
Sediment transport law	Wilcock-Crowe	–
Max erode limit	0.02	m
Active layer thickness	0.1	m
Lateral erosion rate	0.01	–
m value	0.01	–
Water depth threshold for erosion	0.01	m
Evaporation rate	0.0003	m d^{-1}
Courant number	0.4	–
Manning's n	0.04	–

3. Results

3.1. Streamflow

Comparing streamflow between the two extreme spatial rainfall scenarios, the most homogenous (CV = 0.1) and the most heterogeneous (CV = 0.5), reveal that there is a bias toward higher streamflow as rainfall is more heterogeneous, but only for the large flows (higher than 90th percentile, Fig. 5a). Differences in streamflow are also observed for less intense flows but with no clear bias (i.e. distributed evenly around the 1:1 line, Fig. 5a for the streamflow smaller than 90th percentile). Also when visualizing the hydrographs (e.g. Fig. S4), differences between scenarios are mainly apparent in the peak flows.

Quantifying the biases of the low, mean, and peak flows among the different rainfall scenarios confirm the observations made above. For the mean flow, a small positive bias was found between the streamflow emerging from CV = 0.1, 0.3 and 0.5 (median of 1.401 m^3 s^{-1}, 1.403 m^3 s^{-1} and 1.406 m^3 s^{-1}, respectively) but these differences, considering CV = 0.1 as the reference, are very small (<1%, not shown). No change was detected when comparing the low flows emerging from the same CV scenarios (median of 0.038 m^3 s^{-1}, 0.038 m^3 s^{-1} and 0.035 m^3 s^{-1}, respectively). However, for the peak flow, a positive bias (up to 12%) was noticed between the streamflow emerging from CV = 0.1, 0.3 and 0.5 (median of 8.51 m^3 s^{-1}, 9.05 m^3 s^{-1} and 9.56 m^3 s^{-1}, respectively, Fig. 5b). There is a consistency in the influence of rainfall heterogeneity on streamflow.

3.2. Stream morphology

Examining the stream patterns at the end of the simulation (after 300 years) shows differences between the homogeneous (Fig. 6a) and the heterogeneous (Fig. 6b) rainfall scenarios. The impacts of rainfall spatial structure on stream morphology are not uniform and change along with the channel longitudinal profile. Consequently, we analyze the effects of the rainfall spatial structure on stream morphology in four different zones along the mainstream (Fig. 6c): at the watershed head (WH), at the upstream and downstream production areas (P_u and P_d, respectively), and at the alluvial deposition (AD) area next to the outlet of the catchment.

The WH zone is primarily influenced by sediment erosion and transport, with deposition a minor component. The discrepancies in erosion rates at the WH zone between the rainfall spatial scenarios are small, as can be seen comparing the stream profiles A and B (Fig. S5) and in Fig. 6c. In P_u zone, the increase in heterogeneity of rainfall leads to a smaller vertical incision and larger lateral erosion that is expressed in a widening of the mainstream (profile C in Fig. S5 and Fig. 6c). In contrast,

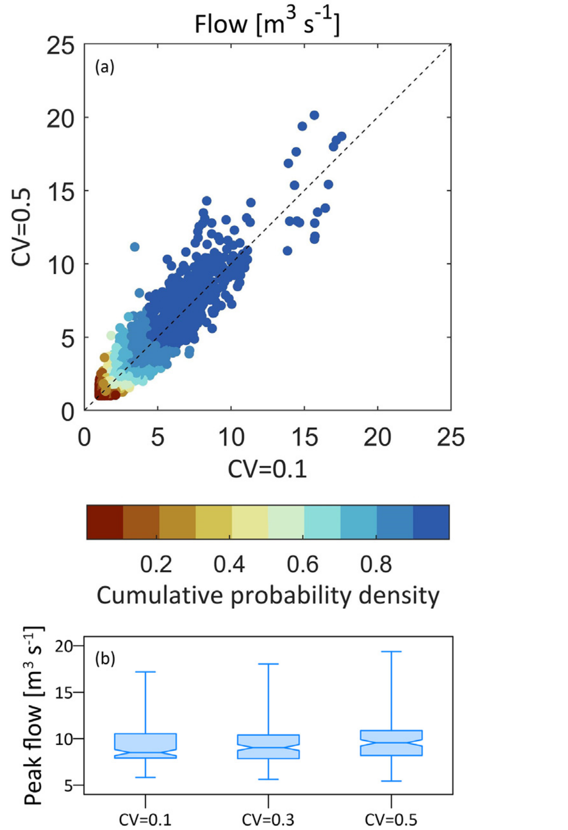

Fig. 5. (a) A cumulative probability distribution of daily streamflow larger than 1 $m^3 s^{-1}$ for the most homogenous and most heterogeneous spatial rainfall scenarios (CV = 0.1 and CV = 0.5, respectively; n = 11,608). (b) Boxplots representing the maximum annual daily streamflow for 150 years (centre line is the median, box edges are the quartiles, and whiskers are the 1–99th percentiles).

the increase in rainfall heterogeneity in P_d zone causes a deeper incision and a smaller widening of the mainstream (Fig. 6c). The magnitude of differences in stream morphology between the two rainfall scenarios is greater in the P_d zone compared to P_u and WH zones.

In assessing the effects of rainfall spatial pattern on sediment erosion and deposition at the entire watershed, we found that increasing rainfall heterogeneity resulted in a greater erosion area but lesser deposition area (Table 3). There is, however, a distinct pattern in the spatial distribution of the deposition along the virtual catchment (Fig. S6). The smaller deposition area in the scenario with higher rainfall heterogeneity is mainly

Table 3
A summary of the erosion and deposition area and totals after 300 years of simulation.

	CV = 0.1	CV = 0.5	Difference
Net erosion area (km^2)	9.52	10.38	9%
Net deposition area (km^2)	6.38	5.52	−13.5%
Total erosion (10^6 km^3)	11.57	12.31	6.4%
Total deposition (10^6 km^3)	8.38	8.98	7.2%

due to the fact that fewer sediment is deposited in P_d. In fact, compared to the homogeneous rainfall scenario, more sediment is produced in P_d and transferred to AD (Fig. 6c) where they are deposited in an alluvial fan that is thicker and laterally extended (Fig. S6).

As shown in Fig. 7, erosion and deposition rates increase linearly as rainfall spatial heterogeneity increases. When comparing the most heterogeneous rainfall scenario to the homogenous one, both erosion and deposition rates increase by up to 55%. Also, in the scenario CV = 0.1, 27.6% of the eroded sediments were transported out of the catchment, while 27% of the eroded sediments were removed from the catchment in the CV = 0.5 scenario. This difference is minor but can indicate that increasing rainfall heterogeneity results in more localized flows that move sediment internally, while more homogeneous rainfall results in more spatially continuous streamflow that are more effective in removing material from a catchment.

3.3. Gully patterns

The effect of the spatial heterogeneity of rainfall on a gully system, composed of main and secondary gullies, was examined for a gully located near the transition point between the upstream and downstream production zones (Fig. 6) at the end of the 300 years of simulation. The main gully is found to be more developed when rainfall is more heterogeneous in space; in general, it is deeper, longer, and with more branches (Fig. 8a–e and Table S2). We note that the main gully can be equally long and developed when comparing two specific rainfall spatial scenarios (e.g. Fig. 8a and d); but even in this case the depth of incision will still be greater for the scenarios with higher rainfall heterogeneity. In contrast to the main gully, the secondary gully is observed to shorten, deepen, and to have fewer branches as rainfall heterogeneity increases (Fig. 8a–e and Table S3).

Examining the whole gully system, it can be seen that rainfall heterogeneity affects the gully pattern (Fig. 8f and Table S4). This is expressed by an increase in the gully vertical incision, the length of the gully system, the number of branches, and by the increasing dominance of the main gully over the secondary gully (Fig. 8f). These changes in gully patterns are most visible when shifting from the homogenous

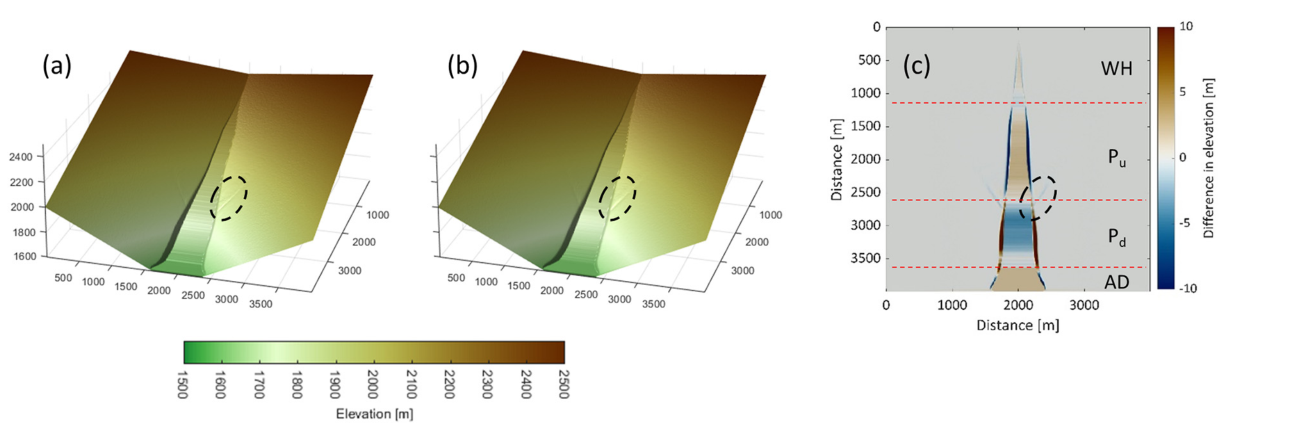

Fig. 6. A plan view of the virtual catchment after 300 years of simulation for the most homogenous (a) and most heterogeneous (b) spatial rainfall scenarios (CV = 0.1 and CV = 0.5, respectively). The difference in elevation between the two scenarios (CV = 0.5–CV = 0.1) is presented in (c). Positive values represent deposition. The channel in (c) is divided into 4 regions: WH — watershed head, P_u — upstream production area, P_d — downstream production area, and AD — alluvial deposition area. The dashed circle points to the gully that is analyzed in Section 3.3.

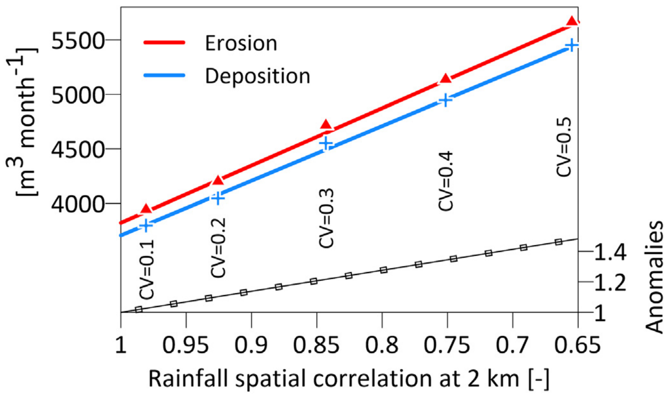

Fig. 7. Erosion (red line) and deposition (blue line) rates as a function of the rainfall spatial scenario. The black line depicts the differences (anomalies) in erosion and deposition rates between the reference scenario (CV = 0.1) and the other rainfall scenarios.

rainfall scenario (CV = 0.1) to the middle-heterogeneous rainfall scenario (CV = 0.3, Fig. 8f); afterwards, it is mainly expressed by the increase in total gully length between the middle-heterogeneous rainfall scenario (CV = 0.3) and most-heterogeneous rainfall scenario (CV = 0.5, Table S4).

It is worth noting that in all rainfall scenarios and model runs the depth to bedrock (minimum depth of 10 m, see Fig. S1) is much deeper than the largest amount of simulated incision, thus erosion and gully development were not limited by the bedrock.

4. Discussion

4.1. Rainfall spatial scenarios

The rainfall spatial scenarios are intended to follow real-world rainfall patterns. Compared to regions mainly affected by stratiform rainfall, those influenced by convective rainfall are expected to display higher levels of heterogeneity as rainfall tends to cluster in multiple smaller but more intense formations (Jaffrain and Berne, 2012; Peleg et al., 2018). Orographic effects may also contribute to the heterogeneity of rainfall in space (Nykanen and Harris, 2003). Examining rainfall patterns at the km scale requires information from a dense rainfall network or weather radars, thus this information is available for only limited locations worldwide. In a literature review, 16 locations were identified that have spatial rainfall information at km and hourly scales (Table 4); these sites are influenced by different types of rainfall and climatic systems. For each of the locations, we associated one of the simulated rainfall spatial scenarios that were used here. This was done using the measure of rainfall spatial correlation at 2-km distance, that was computed for each of the observed locations and for the simulated rainfall scenarios (the match between the CV scenarios and rainfall correlation at 2-km is plotted in Fig. 7). We conclude that the range of spatial rainfall structures observed in nature is covered by our rainfall scenarios. It appears that the most homogeneous and heterogeneous rainfall scenarios are less common in the observed data (only found once for CV = 0.1 and CV = 0.5, Table 4), and that the most common scenario is CV = 0.2 (56% of the total locations, Table 4). However, the locations summarized in Table 4 cover only a tiny portion of the global variability of rainfall spatial structure. Mountainous areas, which play an important role in sediment production, are overlooked in this summary.

Rainfall erosivity is an index assessing the relation between rainfall and erosion (soil loss) by quantifying the kinetic energy of raindrop impact and rate of associated surface runoff. It is computed based on the rainfall energy, considering the rainfall duration, magnitude and intensity (Panagos et al., 2017), but not explicitly the rainfall spatial structure. Plotting rainfall erosivity as a function of rainfall spatial heterogeneity shows a positive correlation between the two components (Fig. 9). This correlation strengthens the results from the numerical experiment, since it demonstrates that the higher erosion we simulate with heterogeneous rainfall agrees with increasing modelled rainfall erosivity rates that are estimated for different locations and climates.

4.2. Rainfall heterogeneity, streamflow and sediment yields

The relationship between rainfall heterogeneity and sediment erosion can be largely explained by surface runoff. Coulthard et al. (2012b) identified a 'geomorphic multiplier' where a change in streamflow results in a nonlinear (cubic) increase in sediment yields. There are two effects of increasing rainfall heterogeneity — an increase in the intensity of the peak rainfall and a clustering of rainfall into smaller areas. Consequently, local streamflow is increasing, generating greater morphological responses. Because of the geomorphic multiplier, these locally larger flows are able to erode and transport more sediment than if those flows were more widely distributed across the catchment. Increased rainfall heterogeneity showed greater streamflow (99th percentile of the maximum annual daily streamflow is 17.1 $m^3\ s^{-1}$, 18 $m^3\ s^{-1}$, and 19 $m^3\ s^{-1}$ for CV = 0.1, 0.3 and 0.5, respectively; Fig. 5b), further enhancing this effect.

4.3. Implications of the results

Our results emphasize the role of the geomorphic multiplier in translating changes in rainfall patterns into a hydro-morphological response. This has important implications for planning for climate change. The full hydro-morphological response from catchments to changing rainfall patterns is still not well understood but non-linear relationships have been shown relating to catchment volumes/intensities (Coulthard et al., 2012b), and spatial distributions (Coulthard and Skinner, 2016; Peleg et al., 2020). Where rainfall is predicted to become more intense and/or more heterogeneous, the landscape will also become more dynamic with increased erosion rates. This has potential implications on sediment delivery downstream and consequently on flood risk (Lane et al., 2007; Slater et al., 2015; Slater, 2016).

The numerical experiment was carried out in a small, synthetic catchment with a controlled rainfall and geological setting. Therefore, we cannot assume the results can be generalized (linearly transferred) to specific catchments and climates. It is reasonable to assume that the hydro-morphological response to the level of heterogeneity of rainfall will be different between locations. For example, arid regions are more likely to be less sensitive to the rainfall spatial structure when comparing two short rainfall events with the same volume of rainfall, as the overland flow is primarily Hortonian (Best et al., 1998), meaning most of the rainfall will be converted to runoff in both scenarios. This natural variability in the hydro-morphological response to the rainfall spatial structure is also apparent from Fig. 9; for instance, in the variability in rainfall erosivity between sites (climates) at decorrelation distances of 0.9. Nevertheless, we expect the trends emerging from the numerical experiment to hold in real catchments, i.e. we predict that higher rainfall heterogeneity will lead to higher erosion and deposition rates, and affect gully development. The numerical experiment demonstrated the fundamental hypothesis that rainfall spatial structure influences the evolution of the landscape at small-scales. Further numerical modelling of real catchments located in different geological regions and different climates is needed to quantify the real-world impacts.

4.4. Geomorphological equifinality

The numerical experiment was confined to 300 years of simulation. Ideally, long-term periods of 10^3–10^4 years (or more) are desirable to capture changes in landscape (Baartman et al., 2013; Tucker and Hancock, 2010). We aimed to simulate the sediment erosion and transport at high spatial resolution (10 m) to identify changes that occurred at the gully scale, which required a long computational time (a month

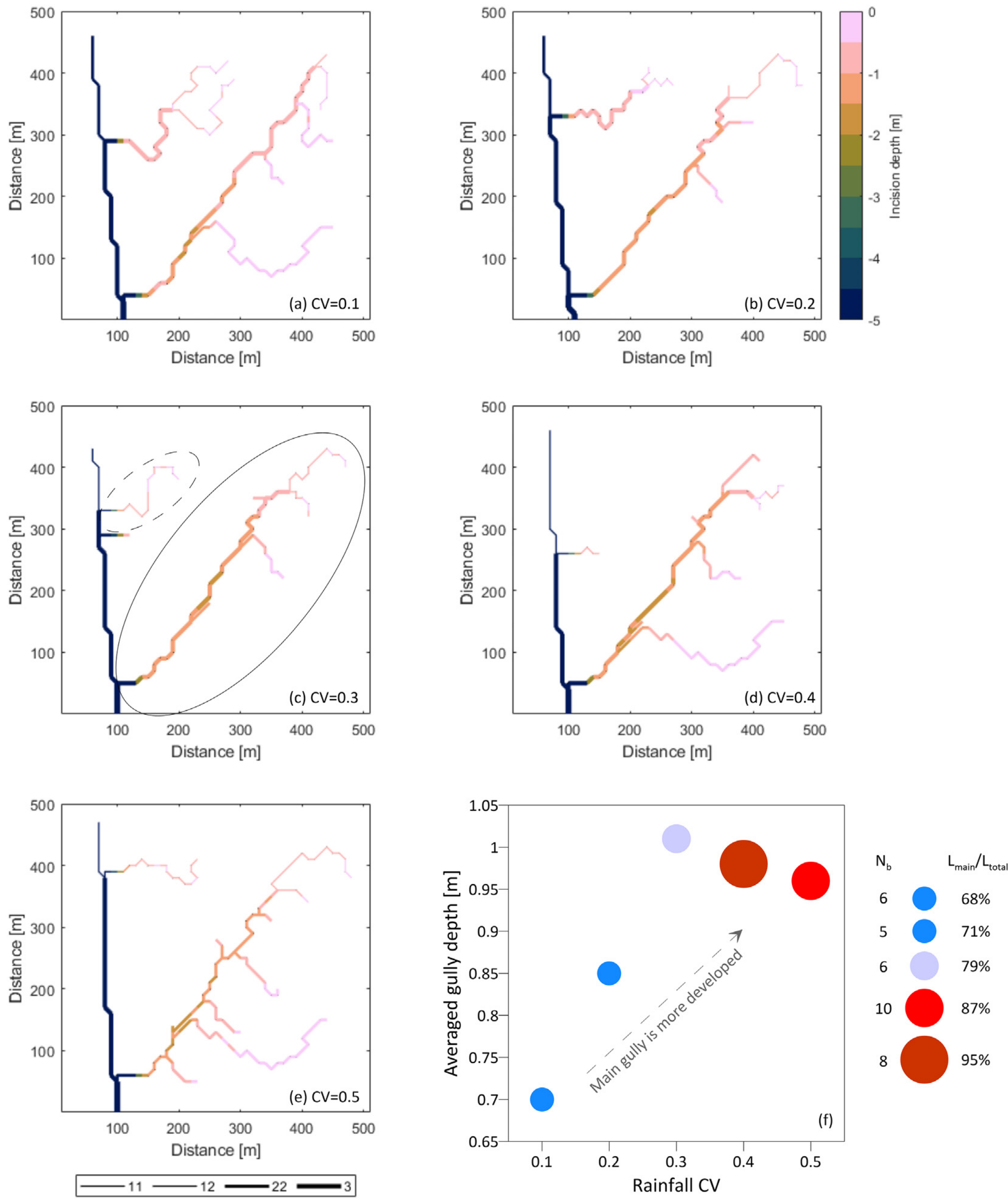

Fig. 8. Maps of the gully patterns (see location in Fig. 6) after 300 years of simulation for the different rainfall spatial scenarios (a–e). The colours of the lines represent the vertical incision depth (bluer means deeper) and the thickness of the lines represents the stream order. The solid-line ellipse in (c) marks the main gully, and the dashed-line ellipse marks the secondary gully. In (f), the averaged depth of the gullies as a function of the rainfall spatial scenario is presented along with the branch numbers of the main gullies (N_b, symbol colour) and the ratio of the lengths between the main gully and the total (L_{main}/L_{total}, symbol size).

per scenario of rainfall using a common desktop). The chosen 300 years is therefore a compromise between the need to simulate long periods and the model running time.

Landscape models are sensitive to 'geomorphological equifinality' (Beven, 1996) issues because their evolution is heavily influenced by the landscape topography itself; thus, these models have the potential to be robust to input uncertainties over long-term simulations (e.g. Hancock et al., 2016; Skinner et al., 2020). This would suggest that while our results indicate considerable changes to the gully development depending on the rainfall spatial structure, given enough time, each of the rainfall spatial scenarios will eventually result in similar changes in the stream pattern. However, this remains an unanswered question since it exceeds our current ability to model landscape evolution at high spatial and temporal resolutions for such long-term periods.

5. Conclusions

A numerical experiment using a virtual catchment and pseudo-climate was conducted to explore the hydro-morphological response to different rainfall spatial scenarios on timescales of hundreds of years. Results demonstrated that both the hydrological and geomorphological components are sensitive to spatial patterns of rainfall. In the rainfall scenarios with a higher degree of spatial heterogeneity, streamflow, erosion and deposition rates were all enhanced and the main gully was found to be more developed. The results also indicate that the influence on the landscape dynamics likely depends on the location along the mainstream, with the production zones being the most sensitive areas to changes in storm properties. All of this suggests that the spatial structure of rainfall may be a significant influence on catchment morphology.

Table 4
A summary of 16 sites with hourly rainfall spatial correlation information. CV [–] refers to the rainfall spatial scenarios simulated here. Rainfall erosivity [MJ mm ha^{-1} h^{-1} y^{-1}] data for each location were obtained from Panagos et al. (2017).

Location	Correlation at 2-km	CV	Rainfall erosivity	Period of observation	Source
Iowa City Municipal Airport, Iowa (US)	0.96	0.1	2700	Apr 1999–Aug 2000	Krajewski et al., 2003
Island of Rota (Guam)	0.91	0.2		May 1998–Jun 1999	Krajewski et al., 2003
Little Washita basin, Oklahoma (US)	0.95	0.2	2900	Jan–May 1999; May–Oct 2001; Mar–Nov 2002	Krajewski et al., 2003; Ciach and Krajewski, 2006; Seo and Krajewski, 2011
Brue catchment (UK)	0.9	0.2	360	Sep 1993–Apr 2000	Villarini et al., 2008
Dalya catchment (Israel)	0.88	0.2	1100	Nov 2011–May 2012	Peleg et al., 2013
Legionowo (Poland)	0.9	0.2	390	Jul 1998–Jun 1999	Moszkowicz, 2000
Arvalis-Institut-du-Végétal (France)	0.9	0.2	1050	Oct 2004–Oct 2005	Moreau et al., 2009
Brunswick (Germany)	0.89	0.2	330	2000–2006	Müller and Haberlandt, 2018
Feldbach (Austria)	0.88	0.2	1100	2007–2016	Schroeer et al., 2018; O and Foelsche, 2019a
Calcasieu Parish, Louisiana (US)	0.9	0.2	6900	Jan 2017–Aug 2018	Sharif et al., 2020
Wallops Island, Virginia (US)	0.87	0.3	2900	Dec 2005–Dec 2007	Tokay and Ozturk, 2012
High Moorsley (UK)	0.86	0.3	290	2007–2010	Rico-Ramirez et al., 2015
Yangtze River Basin (China)	0.81	0.3	4800	Oct 2009–Sep 2011	Li et al., 2014
Melbourne, Florida (US)	0.79	0.4	6800	Aug–Sep 1998	Gebremichael and Krajewski, 2004
Rondonia (Brazil)	0.8	0.4	8000	Jan–Feb 1999	Gebremichael and Krajewski, 2004; Krajewski et al., 2003
Singapore	0.69	0.5	9500	1980–2010	Mandapaka and Qin, 2013

Next steps should involve analysis of hydro-morphological response in catchments located in different climate zones and with different geology, as well as extending the numerical experiment to longer timescales to eliminate equifinality issues. This requires further development of landscape evolution models to enable long-term simulations at a lower computational cost while simulating the response at a high spatial-temporal resolution.

Insights gained in this study have implications not just in the context of landscape evolution, but also in the context of climate impact studies in catchments where changes in the spatial structure of storms may enhance sediment yields and damage infrastructure, such as in-stream structures located in mountainous regions. Therefore, we recommend that the effects of climate change on hydro-morphological systems will go beyond examining changes in rainfall intensity, frequency and timing, which is the common practice, and include changes also to the spatial structure of rainfall.

Supplementary data to this article can be found online at https://doi.org/10.1016/j.geomorph.2021.107863.

Declaration of competing interest

The authors declare that they have no known competing financial interests or personal relationships that could have appeared to influence the work reported in this paper.

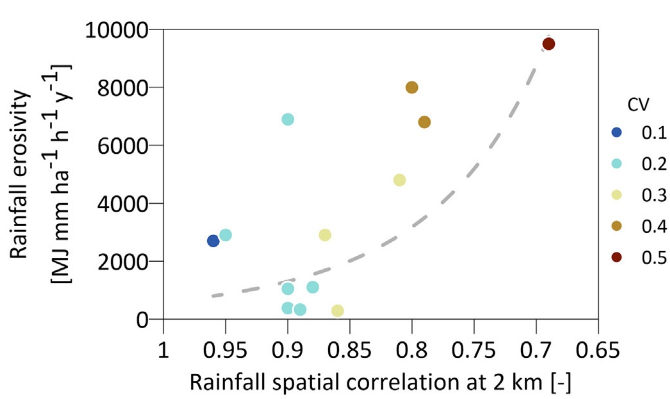

Fig. 9. Rainfall erosivity as a function of the rainfall spatial correlation for selected locations, summarized in Table 4. Symbol colours represent the corresponding spatial rainfall scenarios (CV) simulated here. The dashed line is a power fit [$y = 587x^{-7.6}$] to the data with an R^2 of 0.5.

Acknowledgements

Model results were mostly analyzed using the 'TopoToolBox' (Schwanghart and Scherler, 2014) and many of the figures were plotted using the 'Scientific Colour Maps' (Crameri, 2018). Our thanks go to the reviewers (Jantiene Baartman and an anonymous reviewer) for their suggestions that considerably improved the quality of the manuscript.

References

Abdollahi, K., Guzman, P., Huysmans, M., Batelaan, O., 2016. Rainfall-runoff modelling using a spatially distributed electrical circuit analogue. Nat. Hazards 82 (2), 1279–1300. https://doi.org/10.1007/s11069-016-2243-y.

Acosta-Coll, M., Ballester-Merelo, F., Martinez-Peiro, M., De la Hoz-Franco, E., 2018. Real-time early warning system design for pluvial flash floods—a review. Sensors 18 (7). https://doi.org/10.3390/s18072255.

Baartman, J.E.M., Temme, A., Veldkamp, T., Jetten, V.G., Schoorl, J.M., 2013. Exploring the role of rainfall variability and extreme events in long-term landscape development. Catena 109, 25–38. https://doi.org/10.1016/j.catena.2013.05.003.

Bates, P.D., Horritt, M.S., Fewtrell, T.J., 2010. A simple inertial formulation of the shallow water equations for efficient two-dimensional flood inundation modelling. J. Hydrol. 387 (1–2), 33–45. https://doi.org/10.1016/j.jhydrol.2010.03.027.

Best, E., Herschy, R.W., Herschy, R.W., Gâştescu, P., Starosolsky, Ö., Hughes, D.A., Kolb, C.R., Herschy, R.W., Nicholson, S.E., 1998. Desert hydrology. In: Herschy, R.W., Fairbridge, R.W. (Eds.), Encyclopedia of Hydrology and Water Resources. Springer Netherlands, Dordrecht, pp. 176–183 https://doi.org/10.1007/978-1-4020-4497-7_59.

Beven, K., 1996. 12 Equifinality and uncertainty in geomorphological modelling. The Scientific Nature of Geomorphology: Proceedings of the 27th Binghamton Symposium in Geomorphology, Held 27–29 September 1996. John Wiley & Sons.

Beven, K.J., Kirkby, M.J., 1979. A physically based, variable contributing area model of basin hydrology/Un modèle à base physique de zone d'appel variable de l'hydrologie du bassin versant. Hydrol. Sci. Bull. 24 (1), 43–69. https://doi.org/10.1080/02626667909491834.

Borga, M., Stoffel, M., Marchi, L., Marra, F., Jakob, M., 2014. Hydrogeomorphic response to extreme rainfall in headwater systems: flash floods and debris flows. J. Hydrol. 518, 194–205. https://doi.org/10.1016/j.jhydrol.2014.05.022.

Chang, C.L., 2007. Influence of moving rainstorms on watershed responses. Environ. Eng. Sci. 24 (10), 1353–1360. https://doi.org/10.1089/ees.2006.0220.

Ciach, G.J., Krajewski, W.F., 2006. Analysis and modeling of spatial correlation structure in small-scale rainfall in Central Oklahoma. Adv. Water Resour. 29 (10), 1450–1463. https://doi.org/10.1016/j.advwatres.2005.11.003.

Coulthard, T.J., Skinner, C.J., 2016. The sensitivity of landscape evolution models to spatial and temporal rainfall resolution. Earth Surf. Dynam. 4 (3), 757–771. https://doi.org/10.5194/esurf-4-757-2016.

Coulthard, T.J., Van De Wiel, M.J., 2017. Modelling long term basin scale sediment connectivity, driven by spatial land use changes. Geomorphology 277, 265–281. https://doi.org/10.1016/j.geomorph.2016.05.027.

Coulthard, T.J., Hancock, G.R., Lowry, J.B.C., 2012a. Modelling soil erosion with a downscaled landscape evolution model. Earth Surf. Process. Landf. 37 (10), 1046–1055. https://doi.org/10.1002/esp.3226.

Coulthard, T.J., Ramirez, J., Fowler, H.J., Glenis, V., 2012b. Using the UKCP09 probabilistic scenarios to model the amplified impact of climate change on drainage basin sediment yield. Hydrol. Earth Syst. Sci. 16 (11), 4401–4416. https://doi.org/10.5194/hess-16-4401-2012.

Coulthard, T.J., Neal, J.C., Bates, P.D., Ramirez, J., de Almeida, G.A.M., Hancock, G.R., 2013. Integrating the LISFLOOD-FP 2D hydrodynamic model with the CAESAR model:

implications for modelling landscape evolution. Earth Surf. Process. Landf. 38 (15), 1897–1906. https://doi.org/10.1002/esp.3478.
Crameri, F., 2018. Geodynamic diagnostics, scientific visualisation and StagLab 3.0. Geosci. Model Dev. 11 (6), 2541–2562. https://doi.org/10.5194/gmd-11-2541-2018.
Cristiano, E., ten Veldhuis, M.C., van De Giesen, N., 2017. Spatial and temporal variability of rainfall and their effects on hydrological response in urban areas — a review. Hydrol. Earth Syst. Sci. 21 (7), 3859–3878. https://doi.org/10.5194/hess-21-3859-2017.
Dodov, B., Foufoula-Georgiou, E., 2005. Incorporating the spatio-temporal distribution of rainfall and basin geomorphology into nonlinear analyses of streamflow dynamics. Adv. Water Resour. 28 (7), 711–728. https://doi.org/10.1016/j.advwatres.2004.12.013.
Fekete, B.M., Vorosmarty, C.J., Roads, J.O., Willmott, C.J., 2004. Uncertainties in precipitation and their impacts on runoff estimates. J. Clim. 17 (2), 294–304. https://doi.org/10.1175/1520-0442(2004)017<0294:Uipati>2.0.Co;2.
Gallart, F., Balasch, J.C., Regues, D., Soler, M., Castelltort, X., 2005. Catchment dynamics in a Mediterranean mountain environment: the Vallcebre research basins (southeastern Pyrenees) II: temporal and spatial dynamics of erosion and stream sediment transport. In: Garcia, C., Batalla, R.J. (Eds.), Catchment Dynamics and River Processes: Mediterranean and Other Climate Regions. Developments in Earth Surface Processes, pp. 17–29.
Gayer, E., Michon, L., Louvat, P., Gaillardet, J., 2019. Storm-induced precipitation variability control of long-term erosion. Earth Planet. Sci. Lett. 517, 61–70. https://doi.org/10.1016/j.epsl.2019.04.003.
Gebremichael, M., Krajewski, W.F., 2004. Assessment of the statistical characterization of small-scale rainfall variability from radar: analysis of TRMM ground validation datasets. J. Appl. Meteorol. 43 (8), 1180–1199. https://doi.org/10.1175/1520-0450(2004)043<1180:Aotsco>2.0.Co;2.
Guthrie, R.H., Mitchell, S.J., Lanquaye-Opoku, N., Evans, S.G., 2010. Extreme weather and landslide initiation in coastal British Columbia. Q. J. Eng. Geol. Hydrogeol. 43 (4), 417–428. https://doi.org/10.1144/1470-9236/08-119.
Guzzetti, F., Peruccacci, S., Rossi, M., Stark, C.P., 2008. The rainfall intensity-duration control of shallow landslides and debris flows: an update. Landslides 5 (1), 3–17. https://doi.org/10.1007/s10346-007-0112-1.
Hancock, G.R., 2009. A catchment scale assessment of increased rainfall and storm intensity on erosion and sediment transport for Northern Australia. Geoderma 152 (3–4), 350–360. https://doi.org/10.1016/j.geoderma.2009.07.003.
Hancock, G.R., 2012. Modelling stream sediment concentration: an assessment of enhanced rainfall and storm frequency. J. Hydrol. 430, 1–12. https://doi.org/10.1016/j.jhydrol.2012.01.022.
Hancock, G.R., Coulthard, T.J., 2012. Channel movement and erosion response to rainfall variability in southeast Australia. Hydrol. Process. 26 (5), 663–673. https://doi.org/10.1002/hyp.8166.
Hancock, G.R., Lowry, J.B.C., Coulthard, T.J., Evans, K.G., Moliere, D.R., 2010. A catchment scale evaluation of the SIBERIA and CAESAR landscape evolution models. Earth Surf. Process. Landf. 35 (8), 863–875. https://doi.org/10.1002/esp.1863.
Hancock, G.R., Lowry, J.B.C., Coulthard, T.J., 2015. Catchment reconstruction — erosional stability at millennial time scales using landscape evolution models. Geomorphology 231, 15–27. https://doi.org/10.1016/j.geomorph.2014.10.034.
Hancock, G.R., Coulthard, T.J., Lowry, J.B.C., 2016. Predicting uncertainty in sediment transport and landscape evolution — the influence of initial surface conditions. Comput. Geosci. 90, 117–130. https://doi.org/10.1016/j.cageo.2015.08.014.
Hoober, D., Svoray, T., Cohen, S., 2017. Using a landform evolution model to study ephemeral gullying in agricultural fields: the effects of rainfall patterns on ephemeral gully dynamics. Earth Surf. Process. Landf. 42 (8), 1213–1226. https://doi.org/10.1002/esp.4090.
Iverson, R.M., 2000. Landslide triggering by rain infiltration. Water Resour. Res. 36 (7), 1897–1910. https://doi.org/10.1029/2000wr900090.
Jaffrain, J.l., Berne, A., 2012. Quantification of the small-scale spatial structure of the raindrop size distribution from a network of disdrometers. J. Appl. Meteorol. Climatol. 51 (5), 941–953. https://doi.org/10.1175/jamc-d-11-0136.1.
Jones, J.A., Perkins, R.M., 2010. Extreme flood sensitivity to snow and forest harvest, western Cascades, Oregon, United States. Water Resour. Res. 46. https://doi.org/10.1029/2009wr008632.
Kilsby, C.G., Jones, P.D., Burton, A., Ford, A.C., Fowler, H.J., Harpham, C., James, P., Smith, A., Wilby, R.L., 2007. A daily weather generator for use in climate change studies. Environ. Modell. Softw. 22 (12), 1705–1719. https://doi.org/10.1016/j.envsoft.2007.02.005.
Koutsoyiannis, D., Kozonis, D., Manetas, A., 1998. A mathematical framework for studying rainfall intensity-duration-frequency relationships. J. Hydrol. 206 (1–2), 118–135. https://doi.org/10.1016/s0022-1694(98)00097-3.
Krajewski, W.F., Ciach, G.J., Habib, E., 2003. An analysis of small-scale rainfall variability in different climatic regimes. Hydrol. Sci. J. 48 (2), 151–162. https://doi.org/10.1623/hysj.48.2.151.44694.
Lane, S.N., Tayefi, V., Reid, S.C., Yu, D., Hardy, R.J., 2007. Interactions between sediment delivery, channel change, climate change and flood risk in a temperate upland environment. Earth Surf. Process. Landf. 32 (3), 429–446. https://doi.org/10.1002/esp.1404.
Leonarduzzi, E., Molnar, P., 2020. Deriving rainfall thresholds for landsliding at the regional scale: daily and hourly resolutions, normalisation, and antecedent rainfall. Nat. Hazards Earth Syst. Sci. 20 (11), 2905–2919. https://doi.org/10.5194/nhess-20-2905-2020.
Li, Z., Yang, D., Hong, Y., Zhang, J., Qi, Y., 2014. Characterizing spatiotemporal variations of hourly rainfall by gauge and radar in the mountainous Three Gorges Region. J. Appl. Meteorol. Climatol. 53 (4), 873–889. https://doi.org/10.1175/jamc-d-13-0277.1.
Mandapaka, P.V., Qin, X., 2013. Analysis and characterization of probability distribution and small-scale spatial variability of rainfall in Singapore using a dense gauge network. J. Appl. Meteorol. Climatol. 52 (12), 2781–2796. https://doi.org/10.1175/jamc-d-13-0115.1.
Marra, F., Nikolopoulos, E.I., Creutin, J.D., Borga, M., 2016. Space-time organization of debris flows-triggering rainfall and its effect on the identification of the rainfall threshold relationship. J. Hydrol. 541, 246–255. https://doi.org/10.1016/j.jhydrol.2015.10.010.
May, D.R., Julien, P.Y., 1998. Eulerian and Lagrangian correlation structures of convective rainstorms. Water Resour. Res. 34 (10), 2671–2683. https://doi.org/10.1029/98wr01531.
Mejia, A.I., Moglen, G.E., 2010. Spatial distribution of imperviousness and the space-time variability of rainfall, runoff generation, and routing. Water Resour. Res. 46. https://doi.org/10.1029/2009wr008568.
Menabde, M., Sivapalan, M., 2001. Linking space-time variability of river runoff and rainfall fields: a dynamic approach. Adv. Water Resour. 24 (9–10), 1001–1014. https://doi.org/10.1016/s0309-1708(01)00038-0.
Merz, R., Bloschl, G., 2003. A process typology of regional floods. Water Resour. Res. 39 (12). https://doi.org/10.1029/2002wr001952.
Montgomery, D.R., Dietrich, W.E., Torres, R., Anderson, S.P., Heffner, J.T., Loague, K., 1997. Hydrologic response of a steep, unchanneled valley to natural and applied rainfall. Water Resour. Res. 33 (1), 91–109. https://doi.org/10.1029/96wr02985.
Moreau, E., Testud, J., Le Bouar, E., 2009. Rainfall spatial variability observed by X-band weather radar and its implication for the accuracy of rainfall estimates. Adv. Water Resour. 32 (7), 1011–1019. https://doi.org/10.1016/j.advwatres.2008.11.007.
Morin, E., Goodrich, D.C., Maddox, R.A., Gao, X.G., Gupta, H.V., Sorooshian, S., 2006. Spatial patterns in thunderstorm rainfall events and their coupling with watershed hydrological response. Adv. Water Resour. 29 (6), 843–860. https://doi.org/10.1016/j.advwatres.2005.07.014.
Moszkowicz, S., 2000. Small-scale structure of rain field — preliminary results basing on a digital gauge network and on MRL-5 legionowo radar. Phys. Chem. Earth Pt B Hydrol. Oceans Atmos. 25 (10), 933–938. https://doi.org/10.1016/S1464-1909(00)00128-3.
Müller, H., Haberlandt, U., 2018. Temporal rainfall disaggregation using a multiplicative cascade model for spatial application in urban hydrology. J. Hydrol. 556, 847–864. https://doi.org/10.1016/j.jhydrol.2016.01.031.
Nykanen, D.K., Harris, D., 2003. Orographic influences on the multiscale statistical properties of precipitation. J. Geophys. Res. Atmos. 108 (D8). https://doi.org/10.1029/2001JD001518.
O, S., Foelsche, U., 2019a. Assessment of spatial uncertainty of heavy rainfall at catchment scale using a dense gauge network. Hydrol. Earth Syst. Sci. 23 (7), 2863–2875. https://doi.org/10.5194/hess-23-2863-2019.
O, S., Foelsche, U., 2019b. Assessment of spatial uncertainty of heavy rainfall at catchment scale using a dense gauge network. Hydrol. Earth Syst. Sci. 23 (7), 2863–2875. https://doi.org/10.5194/hess-23-2863-2019.
Ochoa-Rodriguez, S., Wang, L.P., Gires, A., Pina, R.D., Reinoso-Rondinel, R., Bruni, G., Ichiba, A., Gaitan, S., Cristiano, E., van Assel, J., Kroll, S., Murla-Tuyls, D., Tisserand, B., Schertzer, D., Tchiguirinskaia, I., Onof, C., Willems, P., ten Veldhuis, M.C., 2015. Impact of spatial and temporal resolution of rainfall inputs on urban hydrodynamic modelling outputs: a multi-catchment investigation. J. Hydrol. 531, 389–407. https://doi.org/10.1016/j.jhydrol.2015.05.035.
Ogden, F.L., Richardson, J.R., Julien, P.Y., 1995. Similarity in catchment response: 2. Moving rainstorms. Water Resour. Res. 31 (6), 1543–1547. https://doi.org/10.1029/95wr00519.
Panagos, P., Borrelli, P., Meusburger, K., Yu, B., Klik, A., Jae Lim, K., Yang, J.E., Ni, J., Miao, C., Chattopadhyay, N., Sadeghi, S.H., Hazbavi, Z., Zabihi, M., Larionov, G.A., Krasnov, S.F., Gorobets, A.V., Levi, Y., Erpul, G., Birkel, C., Hoyos, N., Naipal, V., Oliveira, P.T.S., Bonilla, C.A., Meddi, M., Nel, W., Al Dashti, H., Boni, M., Diodato, N., Van Oost, K., Nearing, M., Ballabio, C., 2017. Global rainfall erosivity assessment based on high-temporal resolution rainfall records. Sci. Rep. 7 (1), 4175. https://doi.org/10.1038/s41598-017-04282-8.
Papalexiou, S.M., Serinaldi, F., 2020. Random fields simplified: preserving marginal distributions, correlations, and intermittency, with applications from rainfall to humidity. Water Resour. Res. 56 (2). https://doi.org/10.1029/2019wr026331.
Paschalis, A., Molnar, P., Fatichi, S., Burlando, P., 2013. A stochastic model for high-resolution space-time precipitation simulation. Water Resour. Res. 49 (12), 8400–8417. https://doi.org/10.1002/2013wr014437.
Paschalis, A., Fatichi, S., Molnar, P., Rimkus, S., Burlando, P., 2014. On the effects of small scale space-time variability of rainfall on basin flood response. J. Hydrol. 514, 313–327. https://doi.org/10.1016/j.jhydrol.2014.04.014.
Peleg, N., Morin, E., 2012. Convective rain cells: radar-derived spatiotemporal characteristics and synoptic patterns over the eastern Mediterranean. J. Geophys. Res. Atmos. 117. https://doi.org/10.1029/2011jd017353.
Peleg, N., Ben-Asher, M., Morin, E., 2013. Radar subpixel-scale rainfall variability and uncertainty: lessons learned from observations of a dense rain-gauge network. Hydrol. Earth Syst. Sci. 17 (6), 2195–2208. https://doi.org/10.5194/hess-17-2195-2013.
Peleg, N., Blumensaat, F., Molnar, P., Fatichi, S., Burlando, P., 2017a. Partitioning the impacts of spatial and climatological rainfall variability in urban drainage modeling. Hydrol. Earth Syst. Sci. 21 (3), 1559–1572. https://doi.org/10.5194/hess-21-1559-2017.
Peleg, N., Fatichi, S., Paschalis, A., Molnar, P., Burlando, P., 2017b. An advanced stochastic weather generator for simulating 2-D high-resolution climate variables. J. Adv. Model. Earth Syst. 9 (3), 1595–1627. https://doi.org/10.1002/2016ms000854.
Peleg, N., Marra, F., Fatichi, S., Molnar, P., Morin, E., Sharma, A., Burlando, P., 2018. Intensification of convective rain cells at warmer temperatures observed from high-resolution weather radar data. J. Hydrometeorol. 19 (4), 715–726. https://doi.org/10.1175/jhm-d-17-0158.1.

Peleg, N., Molnar, P., Burlando, P., Fatichi, S., 2019. Exploring stochastic climate uncertainty in space and time using a gridded hourly weather generator. J. Hydrol. 571, 627–641. https://doi.org/10.1016/j.jhydrol.2019.02.010.

Peleg, N., Skinner, C., Fatichi, S., Molnar, P., 2020. Temperature effects on the spatial structure of heavy rainfall modify catchment hydro-morphological response. Earth Surf. Dynam. 8 (1), 17–36. https://doi.org/10.5194/esurf-8-17-2020.

Pelletier, J.D., Turcotte, D.L., 2000. Shapes of river networks and leaves: are they statistically similar? Philos. Trans. Royal Soc. Lond. Ser. B Biol. Sci. 355 (1394), 307–311. https://doi.org/10.1098/rstb.2000.0566.

Prein, A.F., Langhans, W., Fosser, G., Ferrone, A., Ban, N., Goergen, K., Keller, M., Tolle, M., Gutjahr, O., Feser, F., Brisson, E., Kollet, S., Schmidli, J., van Lipzig, N.P.M., Leung, R., 2015. A review on regional convection-permitting climate modeling: demonstrations, prospects, and challenges. Rev. Geophys. 53 (2), 323–361. https://doi.org/10.1002/2014rg000475.

Prein, A.F., Rasmussen, R.M., Ikeda, K., Liu, C.H., Clark, M.P., Holland, G.J., 2017. The future intensification of hourly precipitation extremes. Nat. Clim. Change 7 (1), 48 +. https://doi.org/10.1038/nclimate3168.

Rico-Ramirez, M.A., Liguori, S., Schellart, A.N.A., 2015. Quantifying radar-rainfall uncertainties in urban drainage flow modelling. J. Hydrol. 528, 17–28. https://doi.org/10.1016/j.jhydrol.2015.05.057.

Robinson, J.S., Sivapalan, M., 1997. Temporal scales and hydrological regimes: implications for flood frequency scaling. Water Resour. Res. 33 (12), 2981–2999. https://doi.org/10.1029/97wr01964.

Salvadori, G., De Michele, C., 2006. Statistical characterization of temporal structure of storms. Adv. Water Resour. 29 (6), 827–842. https://doi.org/10.1016/j.advwatres.2005.07.013.

Schroeer, K., Kirchengast, G., O, S., 2018. Strong dependence of extreme convective precipitation intensities on gauge network density. Geophys. Res. Lett. 45 (16), 8253–8263. https://doi.org/10.1029/2018GL077994.

Schwanghart, W., Scherler, D., 2014. Short communication: TopoToolbox 2-MATLAB-based software for topographic analysis and modeling in Earth surface sciences. Earth Surf. Dynam. 2 (1), 1–7. https://doi.org/10.5194/esurf-2-1-2014.

Semenov, M.A., Barrow, E.M., 1997. Use of a stochastic weather generator in the development of climate change scenarios. Clim. Chang. 35 (4), 397–414. https://doi.org/10.1023/a:1005342632279.

Seo, B.-C., Krajewski, W.F., 2011. Investigation of the scale-dependent variability of radar-rainfall and rain gauge error covariance. Adv. Water Resour. 34 (1), 152–163. https://doi.org/10.1016/j.advwatres.2010.10.006.

Sharif, R.B., Habib, E.H., ElSaadani, M., 2020. Evaluation of radar-rainfall products over coastal Louisiana. Remote Sens. 12 (9). https://doi.org/10.3390/rs12091477.

Singer, M.B., Michaelides, K., Hobley, D.E.J., 2018. STORM 1.0: a simple, flexible, and parsimonious stochastic rainfall generator for simulating climate and climate change. Geosci. Model Dev. 11 (9), 3713–3726. https://doi.org/10.5194/gmd-11-3713-2018.

Singh, V.P., 1997. Effect of spatial and temporal variability in rainfall and watershed characteristics on stream flow hydrograph. Hydrol. Process. 11 (12), 1649–1669. https://doi.org/10.1002/(SICI)1099-1085(19971015)11:12<1649::AID-HYP495>3.0.CO;2-1.

Sivapalan, M., Bloschl, G., 1998. Transformation of point rainfall to areal rainfall: intensity-duration frequency curves. J. Hydrol. 204 (1–4), 150–167. https://doi.org/10.1016/s0022-1694(97)00117-0.

Skinner, C.J., Peleg, N., Quinn, N., Coulthard, T.J., Molnar, P., Freer, J., 2020. The impact of different rainfall products on landscape modelling simulations. Earth Surf. Process. Landf. 45 (11), 2512–2523. https://doi.org/10.1002/esp.4894.

Slater, L.J., 2016. To what extent have changes in channel capacity contributed to flood hazard trends in England and Wales? Earth Surf. Process. Landf. 41 (8), 1115–1128. https://doi.org/10.1002/esp.3927.

Slater, L.J., Singer, M.B., Kirchner, J.W., 2015. Hydrologic versus geomorphic drivers of trends in flood hazard. Geophys. Res. Lett. 42 (2), 370–376. https://doi.org/10.1002/2014GL062482.

Struthers, I., Sivapalan, M., Hinz, C., 2007. Conceptual examination of climate-soil controls upon rainfall partitioning in an open-fractured soil: I. Single storm response. Adv. Water Resour. 30 (3), 505–517. https://doi.org/10.1016/j.advwatres.2006.04.006.

Tarolli, P., Borga, M., Chang, K.T., Chiang, S.H., 2011. Modeling shallow landsliding susceptibility by incorporating heavy rainfall statistical properties. Geomorphology 133 (3–4), 199–211. https://doi.org/10.1016/j.geomorph.2011.02.033.

Tokay, A., Ozturk, K., 2012. An experimental study of the small-scale variability of rainfall. J. Hydrometeorol. 13 (1), 351–365. https://doi.org/10.1175/jhm-d-11-014.1.

Tokunaga, E., 1978. Consideration on the composition of drainage networks and their evolution. Geogr. Rep. Tokyo Metrop. Univ. 13, 1–27.

Tucker, G.E., Bras, R.L., 2000. A stochastic approach to modeling the role of rainfall variability in drainage basin evolution. Water Resour. Res. 36 (7), 1953–1964. https://doi.org/10.1029/2000wr900065.

Tucker, G.E., Hancock, G.R., 2010. Modelling landscape evolution. Earth Surf. Process. Landf. 35 (1), 28–50. https://doi.org/10.1002/esp.1952.

Valentin, C., Poesen, J., Li, Y., 2005. Gully erosion: impacts, factors and control. Catena 63 (2–3), 132–153. https://doi.org/10.1016/j.catena.2005.06.001.

Viglione, A., Chirico, G.B., Woods, R., Bloschl, G., 2010. Generalised synthesis of space-time variability in flood response an analytical framework. J. Hydrol. 394 (1–2), 198–212. https://doi.org/10.1016/j.jhydrol.2010.05.047.

Villarini, G., Mandapaka, P.V., Krajewski, W.F., Moore, R.J., 2008. Rainfall and sampling uncertainties: a rain gauge perspective. J. Geophys. Res. Atmos. 113 (D11). https://doi.org/10.1029/2007JD009214.

Villarini, G., Smith, J.A., Baeck, M.L., Sturdevant-Rees, P., Krajewski, W.F., 2010. Radar analyses of extreme rainfall and flooding in urban drainage basins. J. Hydrol. 381 (3–4), 266–286. https://doi.org/10.1016/j.jhydrol.2009.11.048.

Volpi, E., Di Lazzaro, M., Fiori, A., 2013. Analytical modeling of the hydrologic response under moving rainstorms: storm-catchment interaction and resonance. J. Hydrol. 493, 132–139. https://doi.org/10.1016/j.jhydrol.2013.04.025.

van Werkhoven, K., Wagener, T., Reed, P., Tang, Y., 2008. Rainfall characteristics define the value of streamflow observations for distributed watershed model identification. Geophys. Res. Lett. 35 (11). https://doi.org/10.1029/2008GL034162.

Wilcock, P., Crowe, J., 2003. Surface-based transport model for mixed-size sediment. J. Hydraul. Eng. 129 (2), 120–128. https://doi.org/10.1061/(ASCE)0733-9429(2003)129:2(120).

Wilks, D.S., Wilby, R.L., 1999. The weather generation game: a review of stochastic weather models. Progr. Phys. Geogr. Earth Environ. 23 (3), 329–357. https://doi.org/10.1191/030913399666525256.

Willems, P., 2000. Compound intensity/duration/frequency-relationships of extreme precipitation for two seasons and two storm types. J. Hydrol. 233 (1–4), 189–205. https://doi.org/10.1016/s0022-1694(00)00233-x.

Xu, X.Z., Liu, Z.Y., Xiao, P.Q., Guo, W.Z., Zhang, H.W., Zhao, C., Yan, Q., 2015. Gravity erosion on the steep loess slope: behavior, trigger and sensitivity. Catena 135, 231–239. https://doi.org/10.1016/j.catena.2015.08.005.

Yakir, H., Morin, E., 2011. Hydrologic response of a semi-arid watershed to spatial and temporal characteristics of convective rain cells. Hydrol. Earth Syst. Sci. 15 (1), 393–404. https://doi.org/10.5194/hess-15-393-2011.

Zhu, Z.H., Wright, D.B., Yu, G., 2018. The impact of rainfall space-time structure in flood frequency analysis. Water Resour. Res. 54 (11), 8983–8998. https://doi.org/10.1029/2018wr023550.